Int. J. Heat Mass Transfer. Vol. 30, No. 10, pp. 1979–1995, 1987
Printed in Great Britain

0017–9310/87 $3.00 + 0.00
Pergamon Journals Ltd.

Heat transfer, pressure drop, and fluid flow patterns in yawed tube banks

A. A. YANEZ MORENO and E. M. SPARROW
Department of Mechanical Engineering, University of Minnesota, Minneapolis, MN 55455, U.S.A.

(*Received* 20 *January* 1987 *and in final form* 3 *April* 1987)

Abstract—Complementary heat transfer, pressure distribution, and flow visualization experiments were performed to investigate the effect of yaw on both staggered and in-line tube tanks. The heat transfer measurements were carried out on a row-by-row basis, and pressures were measured internal to the tube banks as well as upstream and downstream. Air was the heat transfer fluid. The visualization experiments revealed that yaw markedly affected the manner in which the flow impinged on the tubes of the in-line array, with a lesser effect of yaw on the flow field in the staggered array. At a given freestream Reynolds number, the Nusselt number generally decreased as the angle of yaw increased. The yaw effect was well correlated for the staggered array, but not so well for the in-line array because of the aforementioned flow field modifications. The in-line-array Nusselt numbers generally exceeded those for the staggered array, a trend which was accentuated at larger yaw. The pressure drop decreased with increasing yaw. In the present operating range, the in-line-array pressure drops were smaller than the corresponding staggered-array values.

INTRODUCTION

TUBE BANKS are widely used in heat exchange devices. In most applications, the flow external to the tubes approaches the bank in crossflow with respect to the tube axis, so that a substantial literature exists for that configuration. Tube banks that are yawed with respect to the approach flow have heretofore been used sparingly, perhaps due to the absence of sufficient basic data. The present investigation is concerned with yawed tube banks, with the aim of obtaining heat transfer, pressure drop, and flow field information that was not previously available in the literature.

The accessible information for yawed tube banks appears to be limited to that provided by Zukauskas *et al.* [1] and by Groehn [2, 3]. In ref. [1], heat transfer results were presented for the first and fifth rows for tube banks having longitudinal and transverse pitches $\leqslant 1.34D$ (D = tube diameter) and yaw angles between 0 and 65°, but no pressure drop results were given. Groehn's investigation dealt with tube banks having pitches $\leqslant 1.5D$ and yaw angles between 0 and 75°. For a few selected cases, heat transfer results were given on a row-by-row basis, but primary emphasis was placed on the fully developed heat transfer characteristics. The reported pressure drops were measured across the tube bank as a whole (i.e. not on a row-by-row basis).

The present research is a three-part experimental study of yawed tube banks with longitudinal and transverse pitches (both equal to $2D$) larger than those of the previously published work [1–3]. The three parts of the research respectively deal with heat transfer, pressure drop, and pattern of fluid flow. Row-by-row heat transfer measurements were made and, for all the investigated cases, are reported for each of the first seven rows of a nine-row, yawed tube bank. These results are presented so as to highlight both the response of the Nusselt number to the row number (at fixed Reynolds number) and to the Reynolds number (at fixed row number). Special consideration was given to the issue of whether the yaw effect could be correlated by basing the Reynolds number on the component of velocity perpendicular to the tube axis.

Pressure drop experiments were performed for the same cases as for the heat transfer experiments. Pressure measurements were made not only at several axial stations upstream and downstream of the tube bank but also at taps situated in each of the successive rows of the bank. The use of taps within the bank itself is an advance compared with the conventional practice of only using taps situated upstream and downstream of the bank. The in-bank pressure measurements enable the pressure drop per row to be determined without having to be concerned with inlet and exit losses, as in the conventional approach. Both per-row and overall pressure drop results will be presented.

The pattern of fluid flow adjacent to the surfaces of the tubes was made visible by the oil–lampblack technique [4]. The flow visualization was performed at tubes in the first and sixth rows in order to contrast the flow pattern at the inlet of the tube bank with that in the fully developed region. Visualization runs were made at all of the investigated angles of yaw, but only at the highest available Reynolds number of the wind tunnel in order to achieve maximum sharpness of the fluid-flow-induced features in the oil–lampblack surface coating. Illustrative photographs of the visualized flow patterns will be included in the presentation of results.

The experimental work was characterized by four parameters: (1) the longitudinal and transverse

NOMENCLATURE

A	surface area of tube test section
C	coefficient in equation (3)
D	tube diameter
h	per-tube heat transfer coefficient, equation (1)
$K_{E/F}$	dimensionless entrance and exit pressure losses, equation (6)
K_{OV}	dimensionless overall pressure loss, equation (5)
K_{ROW}	dimensionless per-row pressure loss, equation (5)
k	thermal conductivity
N	row number
N_b	number of rows in tube bank
Nu	per-tube Nusselt number, hD/k
Nu_{fd}	fully developed value of Nu
n	exponent in equation (3)
ΔP_{OV}	overall pressure drop
ΔP_{ROW}	per-row pressure drop
p	local pressure
p_∞	atmospheric pressure in laboratory
Q	rate of convective heat transfer at tube test section
Re	freestream Reynolds number, $U_\infty D/\nu$
Re_N	Reynolds number based on velocity normal to tube, $Re \cos\theta$
S_L	longitudinal pitch
S_T	transverse pitch
T_w	test section wall temperature
T_∞	freestream temperature
U_∞	freestream velocity upstream of tube bank.

Greek symbols

ν	kinematic viscosity
θ	angle of yaw ($\theta = 0°$ for crossflow)
ρ	density.

pitches, (2) the angle of yaw, (3) the Reynolds number, and (4) the pattern of tube deployment. As already noted, the longitudinal and transverse pitches were both equal to $2D$. Four angles of yaw were investigated, namely, 0 (crossflow), 15, 30 and 45°. The Reynolds number was based on the freestream velocity well upstream of the tube bank (i.e. the velocity in the unobstructed wind tunnel) and on the tube diameter. The overall range of the Reynolds number extended from about 6500 to 45 000. A separate study was made of staggered and in-line tube banks for all of the aforementioned yaw angles and Reynolds numbers. Both types of arrays were characterized by the same longitudinal and transverse pitches.

The experiments were performed in a low-turbulence (0.4–0.5%), low-speed wind tunnel, so that air served as the heat transfer medium. The temperature difference between the tube wall and the airflow was typically 17–18°C, so that fluid property variations were not a significant factor.

To conserve journal space, it will be necessary to omit many details in the description of the experimental apparatus and procedure and, for the same reason, certain results will have to be left out. All of the omitted information is available in the thesis [5] on which this paper is based. Another source of information is a paper [6] written by the authors on the effect of yaw on heat transfer and fluid flow for a single cylinder.

EXPERIMENTAL APPARATUS

The wind tunnel in which the experiments were performed had a rectangular test section with a cross section of 29.2 × 60.96 cm (width × height) and a 2.4 m length in the flow direction. The tunnel was operated in the open-circuit mode and in suction. In the crossflow configuration, the tubes were oriented vertically. Yaw was attained by inclining the tubes so that the upper end of each tube was situated downstream of the lower end.

The staggered and in-line deployments of the tubes are illustrated in Fig. 1, which shows the forward portions of the respective arrays. Each diagram displays the intersection of a plane parallel to the lower and upper walls of the wind tunnel with the array. For concreteness, the plane may be one of the walls. Owing to the inclination of the tubes, they are cut at an oblique angle by the intersecting plane, yielding an elliptical cross section. The longitudinal and transverse pitches, S_L and S_T, are referred to the aforementioned plane rather than to a plane that is perpendicular to the axes of the inclined tubes. As noted earlier, $S_L/D = S_T/D = 2$.

As can be seen in Fig. 1, there are six tubes in each row. The odd-numbered rows of the staggered array include five whole tubes and two half tubes, one adjacent to each of the side walls of the wind tunnel. The even-numbered rows of the staggered array and all the rows of the in-line array contain only whole tubes. In those rows, the distance between the wall and the center of the nearest tube is $S_T/2$.

The tube banks used for the heat transfer experiments were made up of nine rows, but heat transfer data were collected only in the first seven rows. The eighth and ninth rows served as buffers so that the heat transfer data would not be influenced by hydrodynamic exit effects. For the flow visualization studies, where fluid flow patterns were visualized only in the first and sixth rows, nine-row arrays were also used.

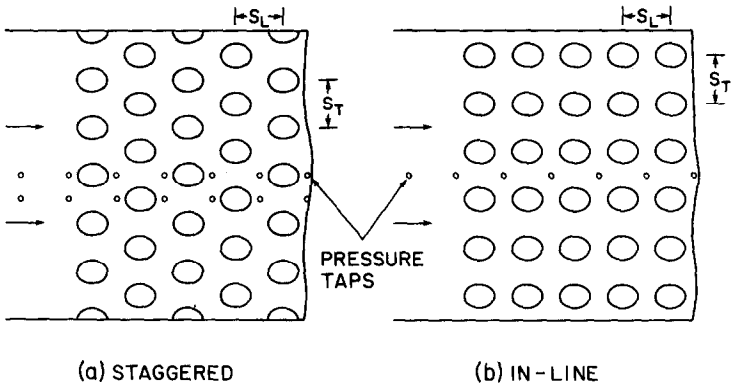

FIG. 1. Layouts of the staggered and in-line arrays.

The pressure drop experiments, which included both in bank measurements and measurements upstream and downstream of the bank, were carried out using eight-row arrays. The slight shortening of the bank for the pressure drop studies was to help accommodate the upstream and downstream taps.

In each heat transfer data run, only one of the tubes was thermally active (i.e. heated), while the other tubes were unheated. The thermally active tube was positioned centrally between the side walls in the particular row selected for study during the given run. The unheated tubes which filled out the bank during the heat transfer runs were also used to populate the arrays used for the pressure drop and flow visualization studies.

The unheated tubes were of relatively simple construction and will be discussed first. Each tube was made from a hollow aluminum cylinder having an outside diameter of 5.08 cm and a 0.3175 cm thick wall. A Delrin (plastic) rod was pressed into each end of the cylinder to partially fill the hollow space. Then, the ends of the assembly were milled flat at 45° to the axis to yield the inclined tube illustrated in Fig. 2(a). The vertical distance between the flat ends was 29.2 cm, just equal to the height of the wind tunnel. Holes were drilled and tapped at the centers of the end faces to facilitate positive attachment of the tube of the bottom and top walls of the wind tunnel.

The just-described fabrication produced tubes suitable for the experiments at a yaw angle of 45°. When all phases of those experiments were completed (heat transfer, pressure drop and flow visualization), the tubes were remachined with the end faces at 60° to the axis, thereby yielding the setup for the 30° angle of yaw. In the machining, the heights of the cylinders were reduced so as to maintain the vertical distance between the flat ends at 29.2 cm. Successive remachinings were performed to obtain the test setups for the 15 and 0° angles of yaw.

The wall-adjacent half tubes for the staggered array were fabricated by the longitudinal cutting of solid aluminum rods. All of the half tubes were unheated.

The thermally active tube was a multicomponent element designed and fabricated to yield controlled thermal boundary conditions, minimal heat losses, and highly accurate measurements of temperature and heat transfer rate. There were, in fact, two versions of the thermally active tube, one of which was used throughout the entire sequence of heat transfer runs, while the second was used for verification runs at the 45° angle of yaw.

The main heat transfer tube is pictured schematically in Fig. 2(b) (the illustrated tube is for the 45° case). As seen there, the tube consisted of a heated test section flanked above and below by a guard heater and by an extension piece the end of which was cut at an angle selected to yield the desired yaw. The test section and the guard heaters were common to all

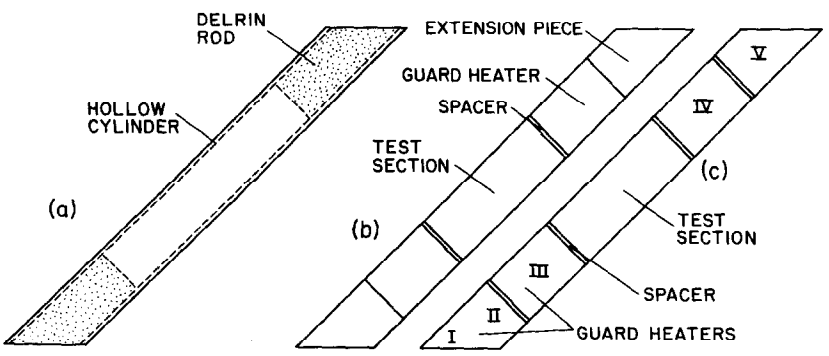

FIG. 2. Side-view diagrams of representative yawed tubes used in the experiments.

the investigated yaws, but the extension pieces were altered in angle and in length for each yaw angle. The tube had an outside diameter of 5.08 cm, and the axial lengths of the test section and of each guard heater were 13.335 and 7.328 cm, respectively. Between the test section and the guard heaters there were 0.3175-cm-thick spacers. The lengths of the extension pieces were chosen so that the vertical height of the assembly would be 29.2 cm.

With a view to ensuring temperature uniformity, the test section and the guard heaters were fabricated with thick-walled external sleeves (0.953 cm thick) from materials with high thermal conductivity (copper and aluminum, respectively). Heating was accomplished by specially fabricated, uniformly wound resistance wire cores which were pressed into the aforementioned thick-walled sleeves and bonded in place with a thermally conducting adhesive. The individual heaters for the test section and for each guard heater were separately controllable.

The test section was instrumented with 15 pre-calibrated, fine-gage chromel–constantan thermocouples. In addition, three thermocouples from the same set were installed in each guard heater at positions aligned with adjacent test section thermocouples. The thermocouple junctions were situated about 0.05 cm from the exposed surface of the tube. This close proximity to the surface obviated the need to correct for possible surface-to-junction temperature differences. A special technique was used for the thermocouple installation [5] which minimized possible perturbations in the wall temperature distribution due to the presence of the thermocouple leads and junction.

During each data run, extraneous conduction losses or gains from the test section were eliminated by matching the temperatures of the test section and the guard heaters. The control of the extraneous transfers was made more sensitive to the temperature matching procedure by the presence of the spacers situated between the test section and the guard heaters. These spacers were made of Delrin plastic (an insulator). The extension pieces were also made of Delrin to reduce conduction losses from the guard heaters.

Extraneous radiation losses from the outer surface of the test section were made negligible by polishing the surface to a mirror finish. The emissivity of the polished surface was measured to be about 0.02, for which the radiation losses were only about 0.2% of the electric power input. The surfaces of the guard heaters were also highly polished.

The yawing of the tubes relative to the freestream flow should give rise to a velocity component along the axes of the tubes. Such an axial flow moving along the surface of the thermally active tube would experience hydrodynamic and thermal boundary layer development prior to its encounter with the heated test section. With this thermal development in mind, there was some concern that the absence of heating at the Delrin extension pieces might possibly affect the heat transfer results at the test section. To deal with this issue, supplementary experiments were performed at the largest angle of yaw (45°) using thermally active extension pieces which enabled the entire tube to be isothermal.

The modified tube is illustrated in Fig. 2(c). As seen there, the Delrin extension pieces were replaced with guard heater sections. Each new guard heater consisted of a thick-walled aluminum sleeve, an individually controlled, custom-wound heater core, and thermocouples. The lower guard heater was actually equipped with two independent heating circuits to enable finer control. This feature was motivated by the expectation that the axial flow would move upward along the tube, thereby washing over the lower portions of the tube before arriving at the test section. All told, there were five guard heaters in the modified version of the thermally active tube, numbered I–V in Fig. 2(c).

For the pressure drop studies, pressure taps were installed in the upper wall of the wind tunnel. The diameter of the tap hole which opened onto the flow was 0.0794 cm. The deployment of the taps in the tube bank is illustrated in Fig. 1. As seen there, the taps were positioned midway between the successive rows, so that the streamwise distance between taps was equal to S_L. Two parallel lines of taps were used in the staggered tube bank, while a single line of taps situated in an open lane between tubes was used in the in-line bank.

Taps were also installed upstream and downstream of the tube bank. There were as many as six taps upstream of the bank. These were successively situated $S_L/2$, $3S_L/2$, $5S_L/2$, $7S_L/2$, $9S_L/2$ and $11S_L/2$ upstream of the center of the first row. Downstream of the bank, taps were positioned $S_L/2$, $3S_L/2$, $5S_L/2$ and $7S_L/2$ from the center of the last row.

The freestream velocity was measured by an impact tube in conjunction with an adjacent wall static tap. The tube and tap were positioned sufficiently far upstream of the bank to avoid the precursive distortions of the flow due to the presence of the bank. Measurements of the impact–static pressure difference and of the static pressure were made with a capacitance-type pressure meter capable of resolving 10^{-3} Torr. The same meter was used for the pressure distribution upstream, within and downstream of the tube bank.

The airstream temperature was measured by a pair of shielded thermocouples suspended in the inter-tube space in the neighborhood of the thermally active tube. The outputs of all thermocouples were read to 1 μV with a digital voltmeter.

FLOW VISUALIZATION

The oil–lampblack technique [4] was used to carry out the flow visualization. The general approach is to apply a thin, uniformly black coating of the oil–

lampblack mixture on the surface which bounds the flow to be visualized. When the airflow is initiated and maintained, the aerodynamic forces acting on the surface will cause a rearrangement of the mixture, giving rise to a pattern of lines, streaks, and dark regions which, when interpreted, reveals the pattern of the fluid flow adjacent to the surface.

The formulation of an oil–lampblack mixture of proper fluidity is essential to the success of the method. A mixture that is too stiff will not respond to the aerodynamic forces, while one that is too fluid will be blown off the surface. When vertical surfaces are involved, as in the present situation, the mixture must be sufficiently stiff so as not to sag under gravity. Another factor is that the aerodynamic forces generally vary across a surface, so that a given mixture may be appropriate for one portion of a surface but not for another portion.

The fluidity of the mixture was varied by varying the relative amounts of oil and lampblack powder and by using oils of different viscosities. The mixture formulation was performed by experience-assisted trial and error, including extensive testing of candidate mixtures. Furthermore, since the clearest visualization patterns were obtained at the highest Reynolds numbers (i.e. which gave rise to the largest aerodynamic forces), all the final visualization runs were carried out for $Re \sim 40\,000$–$45\,000$.

To begin a visualization run, the tube whose adjacent flow pattern was to be examined was covered with a sheet of white, plasticized, self-adhering contact paper, with the seam at the rear of the tube. The oil–lampblack mixture was brushed onto the contact paper so as to form a uniform coating. The coated tube was then installed in the tube bank, after which the airflow was initiated and maintained. Typically, a period of 1–2 h was allowed for the rearrangement of the mixture into a stable pattern. The airflow was then deactivated and the coated tube extracted from the tube bank. The contact paper was then removed from the tube, laid flat, and photographed. Notwithstanding the substantial investment of time and effort and the many repeat runs, all of the final visualization patterns were not of top quality.

All told, patterns for 16 cases are available in ref. [5]. These cases include yaw angles of 0, 15, 30 and 45°, tubes situated in the first and sixth rows of the bank, and staggered and in-line deployment. The first and sixth rows were selected for study to contrast the flow pattern at the inlet of the tube bank with that in the fully developed region.

Space limitations preclude the presentation here of all 16 available visualization patterns. Rather, a representative sample of five patterns will be presented, respectively in Figs. 3–7. Each figure is a photograph taken with the camera positioned perpendicular to the laid-out contact paper. The view presented in the figures is that of an observer who is situated upstream of the tube and is looking downstream at it. For the photographs, part of the separated region on the back side of the tube was masked off because it had been marred by finger marks imprinted during the removal of the contact paper from the tube.

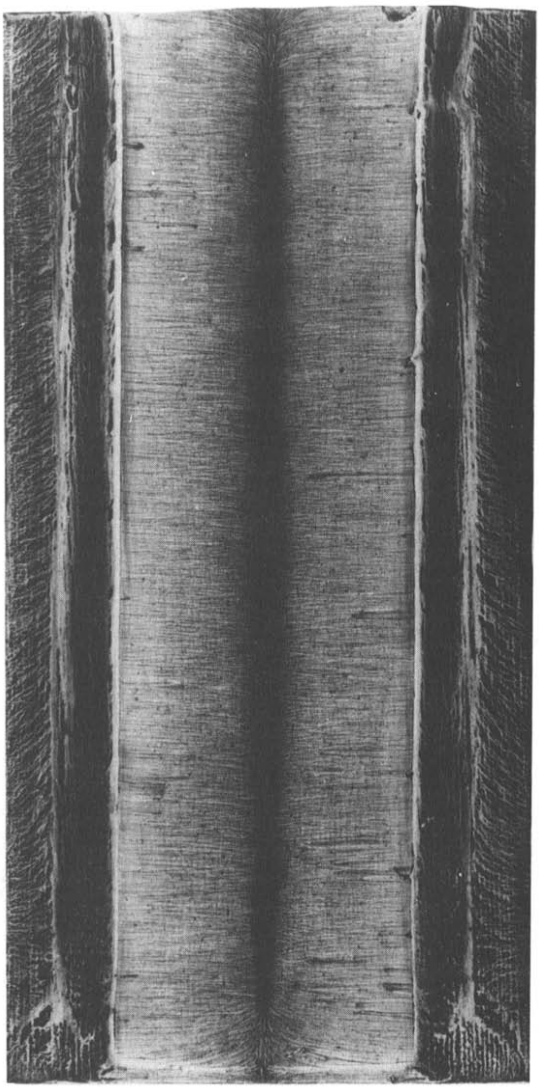

FIG. 3. Flow visualization pattern for the first row of an unyawed staggered or in-line tube bank.

Figure 3 is for the first row of a crossflow tube bank (yaw angles = 0°) and is equally applicable to the staggered and in-line cases. The main features of the visualization pattern are the central, black vertical line, the array of fine streaklines which emanate from the black line, and the broad black bands which flank the streakline region. These features respectively correspond to the forward stagnation line, the boundary layer region on the forward portion of the tube, and the separated region on the rear of the tube.

The fraying of the stagnation line at its lower and upper extremities reflects the end effects due to the wind tunnel walls. These end effects are far removed from the portion of the tube where the test section was situated.

The onset of flow separation occurs at about 90°

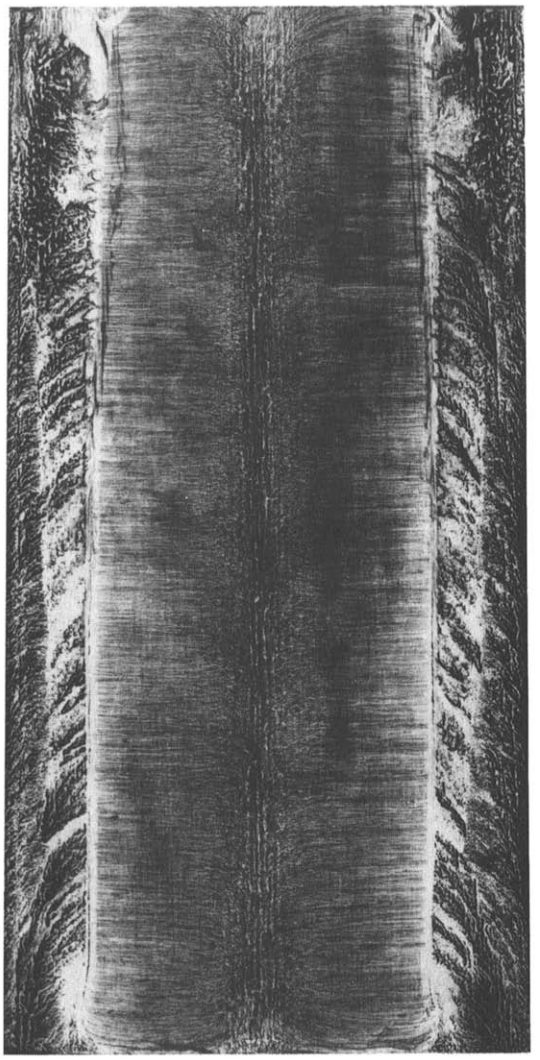

FIG. 4. Flow visualization pattern for the sixth row of an unyawed in-line tube bank.

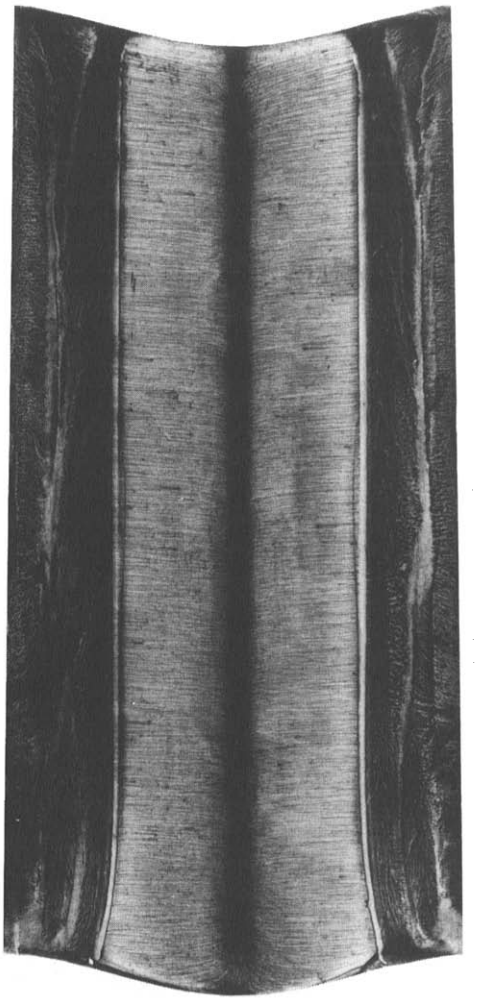

FIG. 5. Flow visualization pattern for the first row of a 15° yawed staggered or in-line tube bank.

from the center of the stagnation line. The initial part of the separated region (dark vertical strip) appears to be washed by a slower-moving recirculating flow than that which washes the remainder of the separated region, where a fine line structure is embedded in a black background.

The visualization pattern for the sixth row in a staggered, non-yawed array closely resembles Fig. 3. However, separation is delayed (103° vs 90°) due to the heightened turbulence, the sluggish portion of the separated region has disappeared, and the end effects are diminished. These features also pertain to the sixth row in an in-line, non-yawed array; however, what is different for the latter is the character of the stagnation line, as can be seen in Fig. 4 (despite the less-than-perfect quality of the visualization).

In an in-line array, in all rows downstream of the first, the throughflow does not impinge directly on the forwardmost portion of a tube. Rather, flow impinges at both sides of the nose of the tube, and there is a recirculation zone between the impinging flows. The central vertical line in evidence in Fig. 4 is not a stagnation line but rather is a manifestation of the aforementioned pocket of recirculating flow.

Figure 5 corresponds to the first row of a 15° yawed tube bank and applies both to the staggered and in-line cases. Since, in the presence of yaw, the contact paper covered both the forward-thrusting lower end of the tube and the rearward-thrusting upper end, its laid-out shape is not a rectangle, as can be seen in the figure. A comparison of Fig. 5 with Fig. 3 shows that the moderate yaw has not caused significant changes. The onset of flow separation continues to occur at about 90° from the forward stagnation line.

For the sixth row of a 15° yawed, staggered array, the main difference relative to the first row is the delay of separation, which now occurs at 110° from the stagnation line. A similar delay of separation is in evidence for the sixth row of a 15° yawed, in-line array. The visualization pattern for the latter case is worth showing (Fig. 6) because it elaborates what was observed in Fig. 4 in the forward portion of the tube.

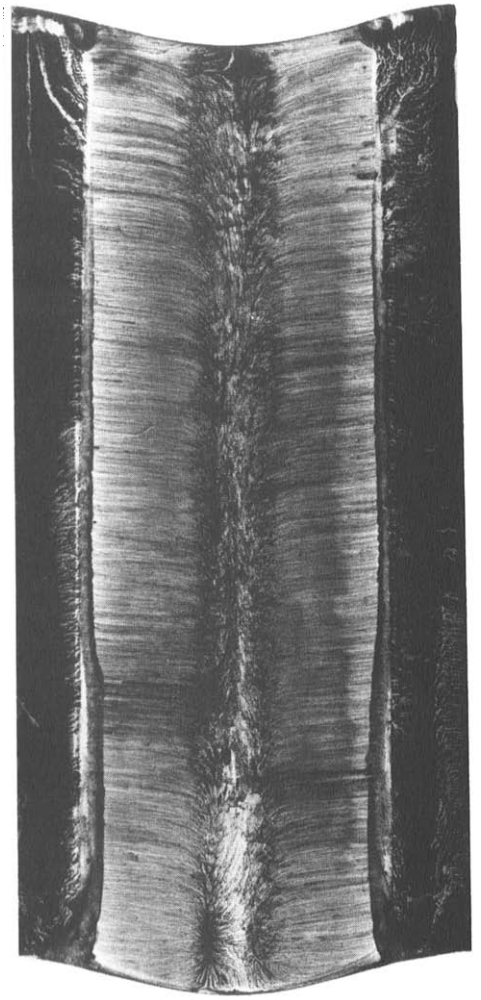

FIG. 6. Flow visualization pattern for the sixth row of a 15° yawed in-line tube bank.

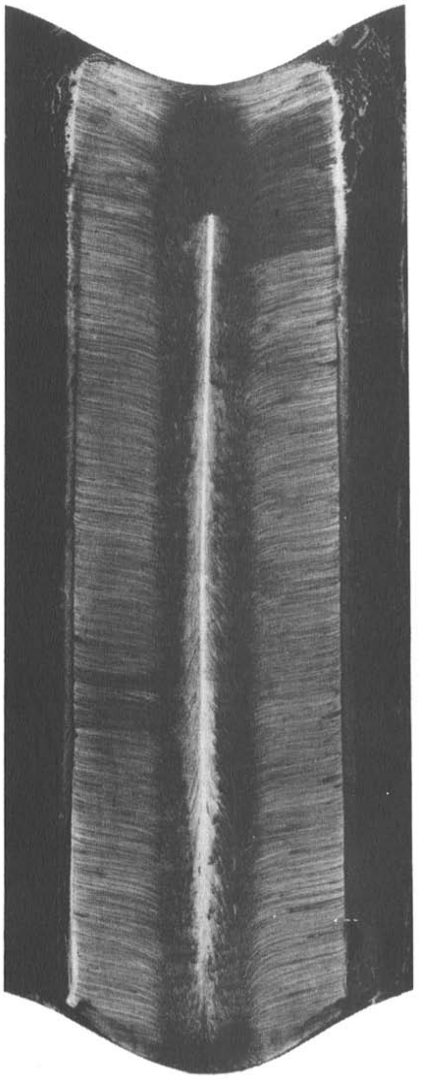

FIG. 7. Flow visualization pattern for the sixth row of a 30° yawed in-line tube bank.

In Fig. 6, the character of the central vertical line is clearly not that of a stagnation line. Rather, it represents the fluid motion in the recirculation zone contained between twin impingements of the mainflow on the tube, the respective impingements being displaced by about 14° from the nose of the tube. By comparing Figs. 6 and 4, it is evident that yaw has increased the displacement of the twin impingements from the nose.

The aforementioned behavior of the flow in the forward region of in-line tubes (beyond the first row) is, perhaps, the most striking finding of the flow visualization, and it is further elaborated in the final photograph, Fig. 7. This figure corresponds to the sixth row of a 30° yawed, in-line array.

As seen there, the twin impingements are displaced still farther from the nose of the tube (i.e. each by 24°), so much so that the individual recirculation zones associated with each impingement are no longer merged. Centered between the recirculation zones is a white vertical line which straddles the nose of the tube. A white region (i.e. the absence of the black mixture) is indicative of a relatively strong flow which blows the mixture off the surface. In particular, in Fig. 7, the white line is created by a flow moving upward along the tube, parallel to the tube axis. Near the upper end of the tube, the axial flow is blocked by the wind tunnel wall and is forced to move to the side. In Fig. 7, the sidewise movement was to the right, as witnessed by the black mixture deposited at that side.

In Fig. 7, separation occurs at about 107° from the nose of the tube, in contrast to the 87° separation in the first row of the 30° yawed tube bank.

Attention may also be drawn to the fact that, owing to yaw, the streaklines of the boundary layer region are not perpendicular to the line which straddles the nose of the tube. As seen in Fig. 7, the streaklines bend toward the perpendicular as they move away from the nose, indicating a decrease in the velocity component parallel to the tube axis.

The photographs for the 45° yawed tube bank reinforce the trends already identified in the foregoing (see ref. [5]).

HEAT TRANSFER RESULTS

Average heat transfer coefficients and Nusselt numbers for the thermally active tube were evaluated from the defining equations

$$h = Q/A(T_w - T_\infty), \quad Nu = hD/k. \tag{1}$$

Here, Q is the rate of convective heat transfer at the test section. The radiation loss was found to be negligible by calculation, while the guard heating eliminated extraneous transfers by conduction. Therefore, Q was equated to the electric power input to the test section heater. The temperatures T_w and T_∞ were evaluated by respectively averaging the wall and freestream thermocouple readings. In general, individual thermocouple readings did not deviate by more than 0.1–0.2% from the average. The quantities A and D represent the surface area and diameter of the test section.

The Reynolds number was based on the freestream velocity U_∞ measured sufficiently far upstream of the tube bank to avoid the precursive distortions of the flow due to the presence of the bank. With this, the Reynolds number was evaluated from

$$Re = U_\infty D/\nu. \tag{2}$$

The thermal conductivity in equation (1) and the kinematic viscosity in equation (2) are those of air at a temperature $(T_w + T_\infty)/2$.

To verify the performance of the experimental apparatus and the validity of the experimental technique, supplementary data runs were carried out using the thermally active tube as a single cylinder in crossflow. The average Nusselt numbers from those experiments are presented in Fig. 2 of ref. [6], where they are compared with the predictions of the Churchill–Bernstein correlation [7]. That correlation is the most recent and, presumably, the most encompassing of the numerous available correlations for the single cylinder case. The deviations between the data and the correlation are typically in the 5% range. These deviations are well within the spread of the literature data on which the correlation is based. On this basis, it can be concluded that the present apparatus and technique are capable of providing data of high accuracy.

Tube bank Nusselt number distributions

The tube bank Nusselt number results will now be presented. For each angle of yaw, the Nusselt numbers are displayed in two complementary figures, each of which shows the results in a different perspective. This presentation format is exemplified by Figs. 8 and 9, which pertain to the no-yaw case, and is repeated in Figs. 10 and 11, 12 and 13, and 14 and 15, which respectively correspond to yaw angles of 15, 30 and 45°.

The first figure in any of the aforementioned pairs conveys the Nusselt number as a function of the Reynolds number. Each such figure is made up of two graphs which separately display the results for the staggered and in-line arrays. In each graph, the data are parameterized by the row number, which ranges from one to seven. If plotted directly, the data for the various rows would tend to overlap. To give a separate identity to the data for each row, the following scheme was adopted: the data for row 1 were plotted directly as Nu, those for the second row were plotted as $Nu \times 1.2, \ldots$, and those for row N were plotted as $Nu \times 1.2^{N-1}$. For each row of each array and for each yaw angle, a power law

$$Nu = C\,Re^n \tag{3}$$

was fit to the data by means of least squares, and these are the straight lines that appear in the figures. In all cases, the data are very well represented by the power-law fit.

In the second figure of each pair, the Nusselt number is plotted as a function of the row number N for parametric values of the Reynolds number. The results for the staggered and in-line arrays are plotted together to facilitate their comparison. Since the actual Reynolds numbers of the experiments deviated somewhat from the targeted values, the Nu vs N plots of Figs. 9, 11, 13 and 15 were obtained by evaluating equation (3) at the Reynolds numbers of choice, i.e. 7000, 13 000, 25 000 and 45 000. Thus, the data symbols appearing in those figures do not represent actual data but rather denote the results obtained from equation (3). Since equation (3) is a very good representation of the data, it was felt that this approach was entirely justified. The data symbols have been interconnected by straight lines to achieve continuity, solid lines for the staggered array, and dashed lines for the in-line array.

Attention is first turned to the Nu–Re presentation of Figs. 8, 10, 12 and 14. Inspection of the staggered-array results of these figures indicates that the Nu–Re lines for $N \geqslant 3$ are separated from each other by a factor close to 1.2, which means that the Nusselt numbers do not vary significantly for rows beyond the third (note the 1.2 multiplying factor for successive rows). However, the separation distances between the row 1 and row 2 results and between the row 2 and row 3 results are substantially greater than a factor of 1.2, indicating sizable row-by-row Nu increases there.

For the in-line array results, the nearly uniform factor of 1.2 spacing of the Nu–Re lines for $N \geqslant 2$ indicates a corresponding row-by-row uniformity of the Nusselt number. Note that in contrast to the staggered array, where significant changes in Nu occurred between the first, second and third rows, such changes occur only between the first and second rows for the in-line array. This observation will be amplified shortly.

The slopes n of the power-law Nu–Re dependence (3) are listed for all cases in Chapter 7 of ref. [5], and only an abbreviated presentation of n values will be made here. In general, for a given yaw angle and a given tube deployment (i.e. staggered or in-line), n at

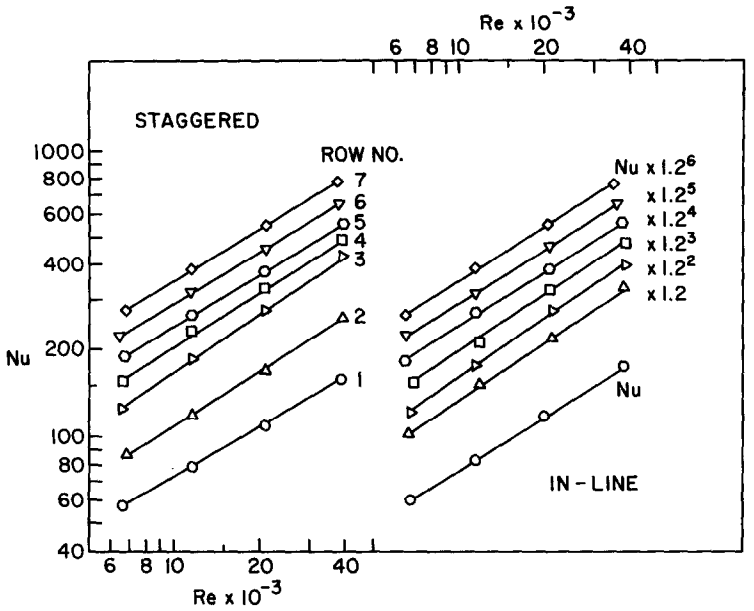

FIG. 8. Variation of Nusselt number with Reynolds number for each row in unyawed staggered and in-line tube banks.

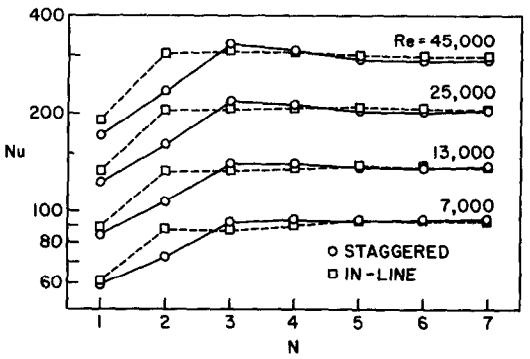

FIG. 9. Variation of Nusselt number with row number in unyawed staggered and in-line tube banks.

first increases with row number, attains a maximum in the neighborhood of $N = 3$, and then decreases and levels off to a constant value. For each case, a trio of n values will be presented: the value for row 1, the maximum value, and the value for row 7. This information is conveyed in Table 1.

From the table, it is seen that the n values are in the neighborhood of 0.65. Aside from a few isolated exceptions, for a given yaw angle, the n values for the in-line array exceed those for the staggered array, indicating that the former array is somewhat more sensitive to the Reynolds number than is the latter. It appears that with increasing yaw, the variation of n with row number diminishes.

Table 1. Representative n values ($Nu = C\,Re^n$)

Yaw angle	Array	n		
		Row 1	Max	Row 7
0	Staggered	0.570	0.674	0.605
0	In-line	0.616	0.678	0.627
15	Staggered	0.586	0.648	0.595
15	In-line	0.605	0.678	0.649
30	Staggered	0.639	0.655	0.609
30	In-line	0.622	0.678	0.650
45	Staggered	0.623	0.648	0.619
45	In-line	0.619	0.677	0.654

A direct comparison of the results for the staggered and in-line arrays is made in Figs. 9, 11, 13 and 15, which display the row-by-row variations of the Nusselt number for parametric values of the Reynolds number. As noted earlier, the main streamwise increase in Nu extends from row 1 to row 3 for the staggered array and from row 1 to row 2 for the in-line array. Another major distinction between the two types of arrays is the presence or absence of overshoot in the Nu vs N distributions, where overshoot denotes the attainment of a maximum or a plateau which exceeds the fully developed value.

The Nu–N distributions for the staggered array definitely display overshoot, the extent of which is heightened as the Reynolds number increases. The presence of the overshoot delays the attainment of fully developed Nu values until either the fifth or sixth rows, depending on the Reynolds number and the yaw angle. For the in-line array, there is no clear evidence of overshoot. Between the second row and the fifth or sixth rows, where fully developed values are attained, Nu is either constant or experiences a modest increase which, in some cases, is punctuated by a slight minimum at row 3.

Note that because there was only one heated tube in the array during a given data run, the attainment of fully developed Nu values was governed only by the hydrodynamic development of the flow. Had thermal development accompanied the hydrodynamic devel-

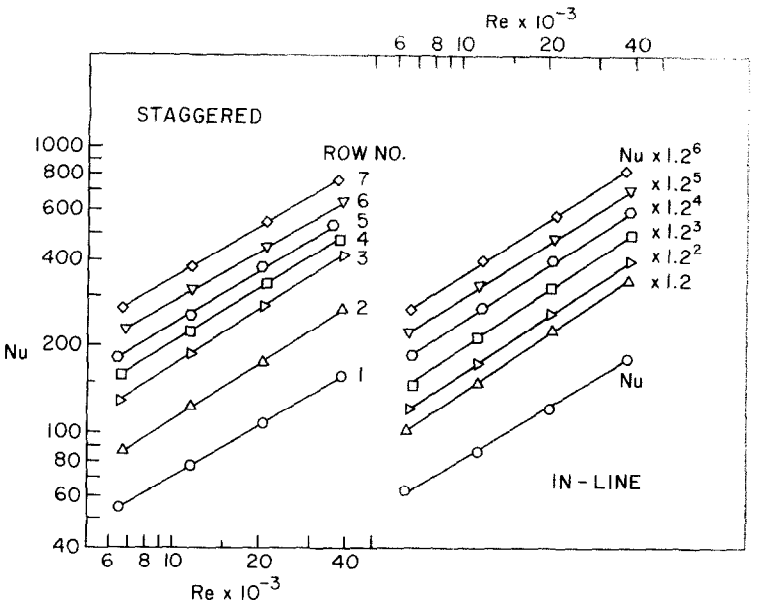

FIG. 10. Variation of Nusselt number with Reynolds number for each row in 15° yawed staggered and in-line tube banks.

opment (i.e. all tubes heated), it is likely that the onset of fully developed Nusselt numbers would have occurred downstream of that encountered here. The magnitudes of the fully developed *Nu* values should be the same with and without simultaneous thermal development.

An overall inspection of Figs. 9, 11, 13 and 15 shows that for the most part, the in-line-array Nusselt numbers exceed those for the staggered array. Only in the region of the overshoot are the staggered-array *Nu* values higher, but even this superiority disappears at higher yaw angles. In general, it appears that the higher yaw angles favor the in-line array. This could well be related to the yaw-related heightened importance of the twin impingements that were observed in the flow visualization studies.

It is relevant to compare the results of Figs. 8–15 to those of the available literature [1–3]. Such a comparison will be qualitative at best because of the sparseness of the literature information and the significant differences in the numerical values of the pitches (i.e. $\leqslant 1.34D$ for ref. [1] and $\leqslant 1.5D$ for refs. [2, 3] ; $2D$ for the present experiments). Indeed, there is too little row-by-row information given in ref. [1], i.e. only for rows 1 and 5, to enable any comparisons to be made.

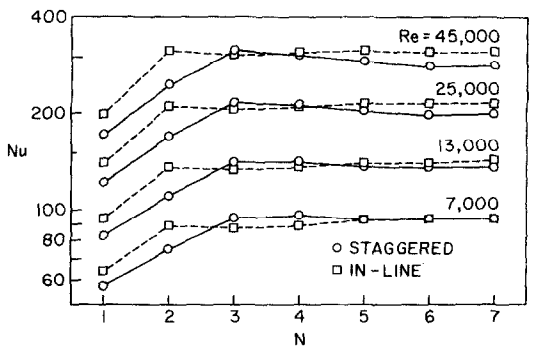

FIG. 11. Variation of Nusselt number with row number in 15° yawed staggered and in-line tube banks.

References [2, 3], although of common authorship, are somewhat conflicting in trend. In ref. [3], there is a single figure which gives the row-by-row Nusselt number distributions for an in-line array at a fixed Reynolds number and for several angles of yaw. That figure shows no overshoot. In ref. [2], there is also one figure devoted to the row-by-row Nusselt number distributions for an in-line array, but there, definite overshoot is in evidence. For the latter figure, the pitches are smaller than those for the former figure, while the Reynolds number is slightly greater. Also in ref. [2] is a figure which gives row-by-row Nusselt numbers for a staggered array characterized by still another pitch. In that figure, there is a slight overshoot. The inconsistent parameterization of the aforementioned figures makes it difficult to discern a trend.

An *Nu–Re* graph in ref. [2] conveying results for successive rows in a yawed, in-line tube bank is in qualitative agreement with what has been presented here. However, power-law fits (i.e. equation (3)) were not obtained in ref. [2], so that the row-by-row variations of the slope n cannot be compared with those found here.

Fully developed tube bank Nusselt numbers

Values of the fully developed Nusselt number Nu_{fd} were determined from the data of Figs. 9, 11, 13 and 15 for the downstream rows. Attention will first be turned to the results for the no-yaw case and their

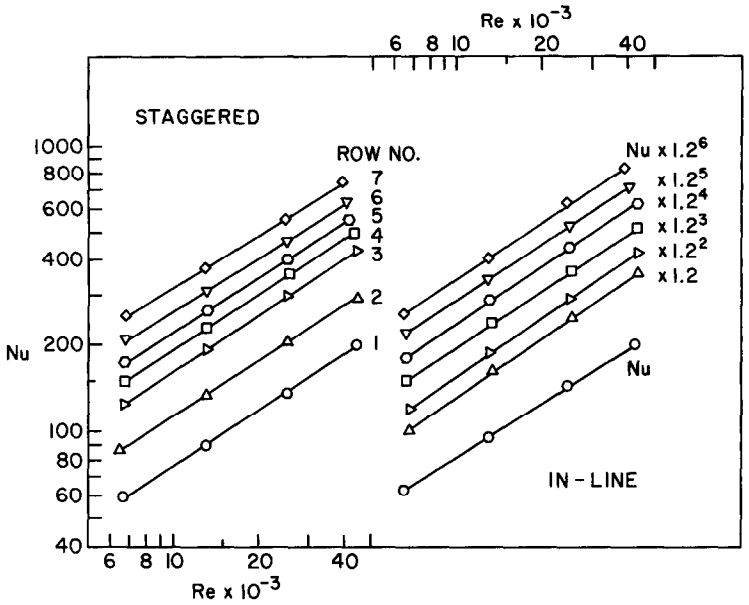

FIG. 12. Variation of Nusselt number with Reynolds number for each row in 30° yawed staggered and in-line tube banks.

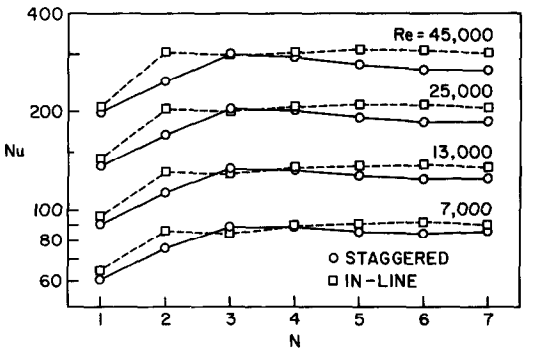

FIG. 13. Variation of Nusselt number with row number in 30° yawed staggered and in-line tube banks.

comparison with the well-established Zukauskas correlation [8]. For the staggered array, the present Nu_{fd} values and those of Zukauskas (in parentheses) are 94.4 (94.6), 137.3 (137.2), 203.8 (203.1) and 290.8 (289.0) for Re = 7000, 13 000, 25 000 and 45 000. The agreement between the two sets of results is excellent (deviations of less than 0.6%). For the in-line array, the corresponding values of Nu_{fd} are 93.4 (97.2), 137.7 (143.5), 207.3 (216.7) and 299.5 (313.9). The deviations between the present results and the Zukauskas correlation are in the 6% range. It is noteworthy that these deviations are smaller than the deviations between the Zukauskas correlation and the data on which it was based. The foregoing comparisons lend further support to the effectiveness of the present experimental apparatus and experimental procedure.

The effect of yaw on the fully developed Nusselt number will now be considered, and Fig. 16 has been prepared for this purpose. In this figure, Nu_{fd} is plotted as a function of the angle of yaw for parametric values of the Reynolds number and for both the staggered and in-line arrays. From the figure, it is seen that, in general, the Nu_{fd} values for the in-line array exceed those for the staggered array. The differences between the two arrays are slight for the no-yaw case but become more significant as both the angle of yaw and the Reynolds number increase. For the parameter ranges of Fig. 16, the largest deviation between the two sets of results is about 35%.

The superiority of the in-line array can be attributed to flow field characteristics which were visualized in Figs. 3–7. In particular, for the in-line array, there was a yaw-related change in the position at which the mainflow impinged on the tubes of the array. These changes bring about superior mixing which is accentuated at higher Reynolds numbers, thereby enhancing the heat transfer.

Figure 16 reveals an interesting difference in the dependence of Nu_{fd} on the yaw angle for the two arrays. For the staggered array, Nu_{fd} decreases monotonically with the yaw angle. This behavior is consistent with the angle-related decrease of the velocity component normal to the tube surface at a fixed value of Re. On the other hand, for the in-line array, there appears to be a local maximum at a yaw angle of about 15°, after which a monotonic decrease occurs. The maximum could well result from the conflict between the angle-related decrease in the normal velocity component and the enhancement due to the angle-related change in the impingement of the mainflow.

For yawed tubes or cylinders, it is common to seek a correlation of the effect of yaw by using a Reynolds number Re_N which is based on the component of the

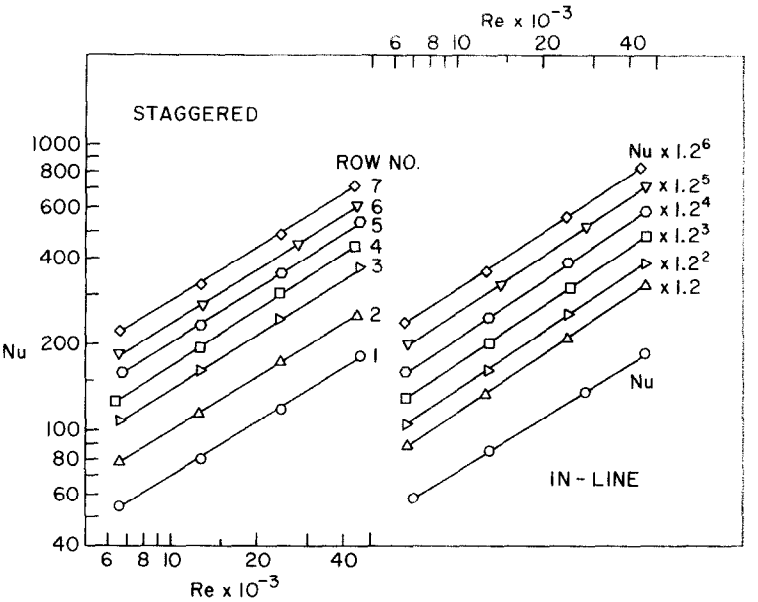

FIG. 14. Variation of Nusselt number with Reynolds number for each row in 45° yawed staggered and in-line tube banks.

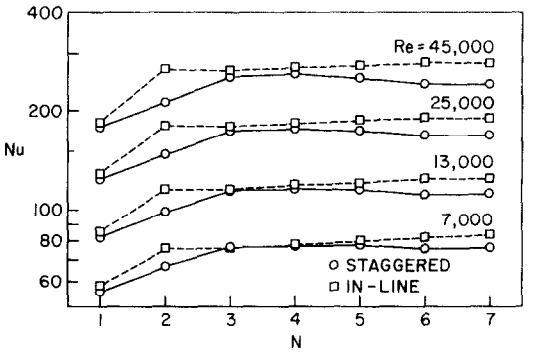

FIG. 15. Variation of Nusselt number with row number in 45° yawed staggered and in-line tube banks.

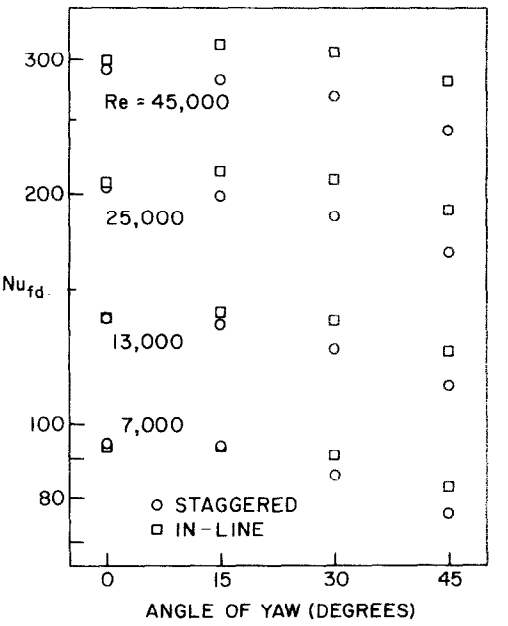

FIG. 16. Effect of yaw on the fully developed Nusselt number.

velocity normal to the surface of the tube. If successful, such a correlation renders Nu_{fd} independent of yaw and is often called the Independence Principle. The relation between Re_N and Re is

$$Re_N = Re \cos \theta \tag{4}$$

where θ is the angle of yaw.

In Fig. 17, Nu_{fd} is plotted as a function of Re_N for the staggered array. The figure contains data for all four investigated yaw angles (0, 15, 30 and 45°). For reference purposes, a straight line has been passed through the 0° data. Examination of the figure indicates a completely successful correlation whereby the data for all the yaw angles are brought together and are coincident with those for the no-yaw case. Thus, the Independence Principle holds for the staggered array.

A corresponding presentation is made in Fig. 18 for the in-line array. It is evident from the figure that there is a systematic deviation of the data from the no-yaw line with increasing yaw and increasing Reynolds number. The deviations are moderate; for example, from 7 to 17% over the investigated range of Reynolds number for the 45° yaw. Nevertheless, it has to be concluded that the Independence Principle does not hold.

From a consideration of the flow visualization results, it is believed that there is ample reason for the non-applicability of the Independence Principle for the in-line array. The visualization revealed significant yaw-angle-related changes in the structure of the flow. Such changes are at variance with the notion that

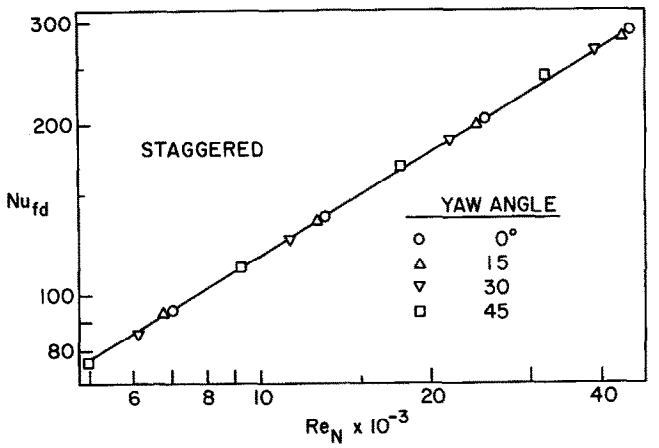

FIG. 17. Correlation of staggered-array fully developed Nusselt numbers with the normal-velocity-based Reynolds number Re_N.

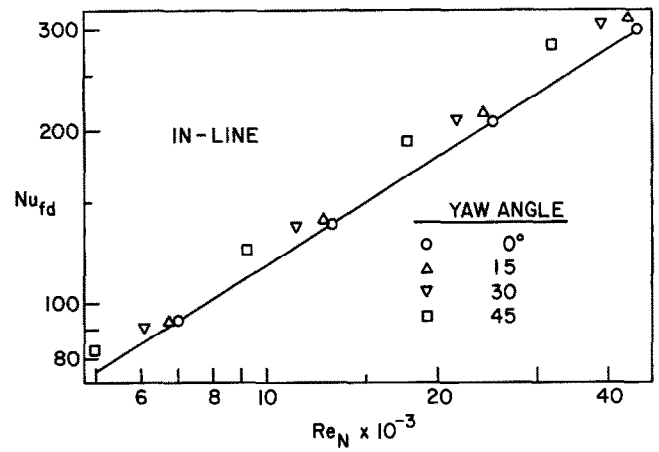

FIG. 18. Correlation of in-line-array fully developed Nusselt numbers with the normal-velocity-based Reynolds number Re_N.

similarity must prevail in the flow field in the presence of varying yaw in order that the Independence Principle hold.

In view of the foregoing, it is surprising that in refs. [2, 3], the Independence Principle was found to be valid for the in-line arrays investigated there. As noted earlier, the tube banks of refs. [2, 3] had significantly smaller pitches than that used here. With regard to the staggered array, ref. [2] indicates a modest deviation from the Independence Principle (~7%), whereas in ref. [3] it is purported to be valid. The results of ref. [1] for both staggered and in-line arrays were also plotted in a manner to display the validity of the Independence Principle. However, data scatter precludes a definitive conclusion.

As a final matter relevant to the heat transfer results, attention is turned to the supplementary experiments that were performed using the heated tube illustrated in Fig. 2(c) instead of that of Fig. 2(b) which was used in obtaining the results presented heretofore. As noted earlier, for the latter, the outboard members (i.e. the extension pieces) were unheated, while for the former, additional guard heaters were installed to make the entire tube isothermal.

A comparison of Nusselt number results obtained using the two types of heated tubes is presented in Fig. 7.17 of ref. [5]. The comparison was made for the first and sixth rows of both the staggered and in-line arrays over the entire investigated Reynolds number range. The yaw angle was 45°. In general, the deviations between the two sets of data were in the 2% range. These deviations are too small to be of practical significance. It may, therefore, be concluded that the results presented here were unaffected by the unheated extension pieces of the heated tube.

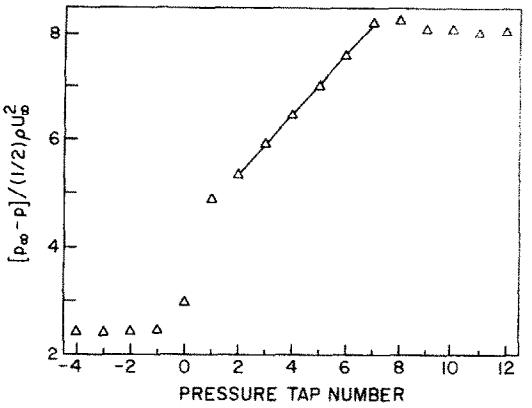

FIG. 19. Representative pressure distribution (eight-row in-line array, yaw angle = 30°, Re = 25 000).

PRESSURE DROP RESULTS

As was noted earlier, the present pressure drop experiments differed from those of conventional tube bank studies in that pressure distributions were measured internal to the bank as well as upstream and downstream of the bank. The upstream and downstream measurements were, themselves, somewhat unusual because numerous longitudinally deployed pressure taps were used.

A representative pressure distribution is shown in Fig. 19. The figure corresponds to Re = 25 000, a yaw angle of 30°, and to the in-line array with eight rows of tubes. On the ordinate, the difference between a reference pressure p_∞ (atmospheric pressure in the laboratory) and the local pressure p is made dimensionless by the velocity head $\rho U_\infty^2/2$. Here, ρ corresponds to the density at a point midway through the array while U_∞ is the freestream velocity far upstream of the tube bank. The abscissa is the pressure tap number.

For the data run depicted in Fig. 19, the tube bank was positioned in the wind tunnel such that tap 0 was situated a distance $S_L/2$ upstream of the center of the first row, with taps −1, −2, −3 and −4 at upstream distances $3S_L/2$, $5S_L/2$, $7S_L/2$, and $9S_L/2$, respectively. Taps 1–7 are within the tube bank as illustrated in Fig. 1(b). Downstream of the bank, taps 8–12 were respectively situated $S_L/2$, $3S_L/2$, $5S_L/2$, $7S_L/2$ and $9S_L/2$ from the center of the last row.

Upstream of the bank, the pressure is virtually constant. The acceleration of the flow to accommodate the partial blockage caused by the tube bank gives rise to a slight precursive pressure drop at tap 0 and a large pressure drop at tap 1. The pressure decreases linearly between taps 2–7, indicating that the flow is periodically fully developed. Just downstream of the bank, there is a slight pressure recovery, after which the pressure is virtually constant.

Dimensionless representations of the overall and per-row pressure drops may be written as

$$K_{OV} = \Delta P_{OV}/(\rho U_\infty^2/2), \quad K_{ROW} = \Delta P_{ROW}/(\rho U_\infty^2/2) \tag{5}$$

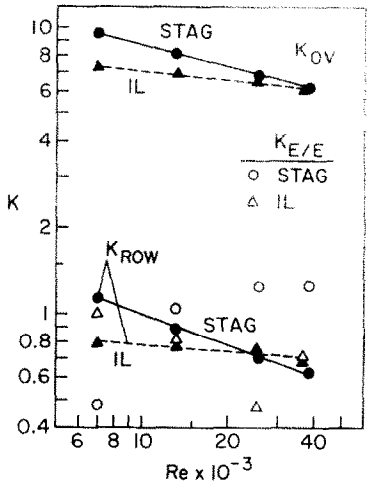

FIG. 20. Overall, per-row, and entrance–exit pressure drops for unyawed staggered and in-line tube banks.

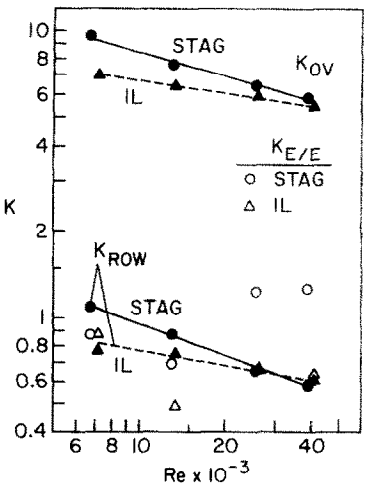

FIG. 21. Overall, per-row, and entrance–exit pressure drops for 15° yawed staggered and in-line tube banks.

in which ΔP_{OV} is the overall pressure drop measured from upstream of the bank to downstream of the bank, and ΔP_{ROW} is the per-row pressure drop in the periodic fully developed regime. The entrance and exit losses were evaluated from

$$K_{E/E} = K_{OV} - N_b K_{ROW} \tag{6}$$

in which N_b is the number of rows in the tube bank.

The pressure drop results in terms of K_{OV}, K_{ROW}, and $K_{E/E}$ are presented in Figs. 20–23, which respectively correspond to yaw angles of 0, 15, 30 and 45°. Each figure conveys results for both the staggered and in-line arrays, respectively represented by the circle and triangle data symbols. The data for K_{OV} and K_{ROW} have been interconnected by straight lines for continuity, while those for $K_{E/E}$ are quite scattered and were, therefore, not interconnected. Note that the results of Figs. 20–23 for K_{OV} correspond to an eight-row array. For tube banks having other than eight rows, it is suggested that K_{OV} be computed from

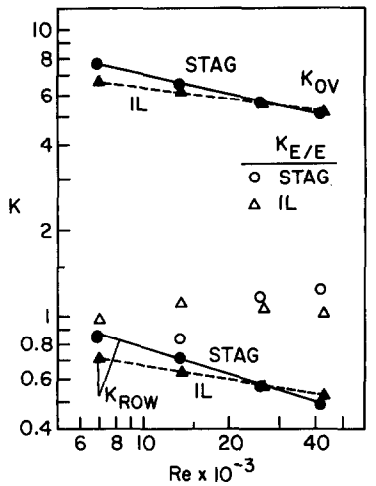

FIG. 22. Overall, per-row, and entrance–exit pressure drops for 30° yawed staggered and in-line tube banks.

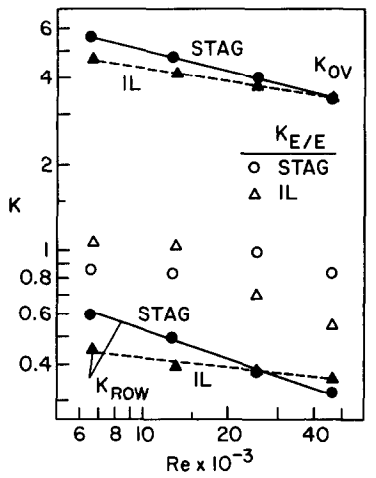

FIG. 23. Overall, per-row, and entrance–exit pressure drops for 45° yawed staggered and in-line tube banks.

$$K_{OV} = (K_{OV})_8 + (N_b - 8)K_{ROW} \quad (7)$$

where $(K_{OV})_8$ is from Figs. 20–23.

The figures show that, in general, the overall pressure drop for the staggered array exceeds that for the in-line array. However, due to the greater downslope of the staggered-array data, the results for the two arrays converge as the Reynolds number increases. It appears that at still larger Reynolds numbers, the in-line-array pressure drop will exceed that for the staggered array. It is also seen that the deviations between the K_{OV} values for the two types of arrays tend to be somewhat smaller at larger yaw than when there is no yaw, especially at the lower *Re*.

It is particularly noteworthy that K_{OV} decreases as the angle of yaw increases, gradually at first and then more rapidly. For the staggered array, the K_{OV} value at 45° yaw is about 58% of that for the no-yaw case, independent of the Reynolds number in the investigated range. For the in-line array, the corresponding percentages are 62, 61, 58 and 57%, respectively for *Re* = 7000, 13000, 25000 and 40000. These results are in good quantitative agreement with those of refs. [2, 3].

For the per-row pressure drop K_{ROW}, there is a crossover in the results for the two arrays due to the different slopes of the respective K_{ROW} vs *Re* dependencies. For the low and intermediate Reynolds numbers in the investigated range, the staggered-array K_{ROW} values exceed those for the in-line array; the opposite relation occurs at the high end of the range. As was the case for K_{OV}, it is also seen that K_{ROW} decreases with increasing yaw, especially at larger angles of yaw.

The fact that both K_{OV} and K_{ROW} decrease with increasing *Re* indicates that as U_∞ increases, the increases in ΔP_{OV} and ΔP_{ROW} are somewhat less than proportional to U_∞^2. A strict proportionality to U_∞^2 (i.e. *K* independent of *Re*) would indicate that the pressure drop is due solely to inertial losses, while the departures from U_∞^2 are indicative of the presence of skin-friction-related pressure drop. Since *K* is less dependent on *Re* for the in-line array than for the staggered array, it may be concluded that the contribution of inertial losses relative to friction losses is greater for the former than for the latter.

The entrance and exit losses $K_{E/E}$ were obtained from the differencing operation indicated in equation (6). The two terms which appear on the right-hand side of equation (6) are of comparable magnitude, so that the differencing gives rise to scatter in $K_{E/E}$, as is evident in Figs. 20–23. Because of the scatter, it is difficult to identify trends in $K_{E/E}$. Typically, $K_{E/E}$ is of the order of $\rho U_\infty^2/2$. In view of the uncertainty associated with the scatter, it is deemed advisable to compute K_{OV} from equation (7), thereby bypassing $K_{E/E}$.

CONCLUDING REMARKS

This paper has reported a three-part experimental study of yawed staggered and in-line tube banks, with the unyawed tube bank included as a reference case. Flow visualization, performed using the oil–lampblack technique, revealed that yaw markedly affected the pattern with which the mainflow in the bank impinged on the tubes of the in-line array. The flow field in the staggered array appeared to be less affected by yaw.

The Nusselt numbers for the in-line tube bank generally exceeded those for the staggered tube bank, a trend which was accentuated at larger yaw angles. At a given freestream Reynolds number, the Nusselt number generally decreased as the yaw angle increased. For the staggered array, the fully developed Nusselt numbers for the yawed tube banks were brought together with those for the no-yaw case using a Reynolds number based on the component of the velocity which is normal to the tubes, yielding the so-called Independence Principle. The Independence Principle was not strictly obeyed for the in-line tube

banks, probably because of the aforementioned yaw-related changes in the pattern of fluid flow.

In the investigated Reynolds number range, the overall pressure drops for the in-line tube banks were smaller than those for staggered tube banks. The pressure drop decreased as the yaw angle increased, gradually at first and then more rapidly.

It is noteworthy that for the cases investigated here, the in-line tube banks displayed higher Nusselt numbers and lower pressure drops than did the staggered tube banks.

REFERENCES

1. A. A. Zukauskas, V. I. Katinas and E. E. Perednis, Average heat transfer coefficients of tube bundles in flows of viscous fluids at different angles of attack, *Heat Transfer–Sov. Res.* **15**(2), 22–30 (1983).
2. H. G. Groehn, Thermal hydraulic investigation of yawed tube bundle heat exchangers. In *Heat Exchangers: Thermal–Hydraulic Fundamentals and Design* (Edited by S. Kakac, A. E. Bergles and F. Mayinger), pp. 97–109. Hemisphere, Washington, DC (1981).
3. H. G. Groehn, Influence of the yaw angle on heat transfer and presure drop of tube bundle heat exchangers, *Proc. 7th Int. Heat Transfer Conference*, Vol. 6, pp. 203–208. Hemisphere, Washington, DC (1982).
4. W. Merzkirch, *Flow Visualization*. Academic Press, New York (1974).
5. A. A. Yanez Moreno, Heat transfer and pressure drop in a tube bank inclined with respect to the flow, Ph.D. thesis, Department of Mechanical Engineering, University of Minnesota, Minneapolis, Minnesota (1985).
6. E. M. Sparrow and A. A. Yanez Moreno, Effect of yaw on forced convection heat transfer from a circular cylinder, *Int. J. Heat Mass Transfer* **30**, 427–435 (1987).
7. S. W. Churchill and M. Bernstein, A correlating equation for forced convection from gases and liquids to a circular cylinder in crossflow, *J. Heat Transfer* **99**, 300–306 (1977).
8. A. A. Zukauskas, Heat transfer from tubes in crossflow. In *Advances in Heat Transfer*, Vol. 8, pp. 93–160. Academic Press, New York (1972).

TRANSFERT THERMIQUE, PERTE DE CHARGE ET CONFIGURATIONS D'ECOULEMENT DANS DES BANCS DE TUBES EN DERAPAGE

Résumé—Des expériences complémentaires de transfert de chaleur, de distribution de pression et de visualisation d'ecoulement précisent l'effet du dérapage sur des bancs de tubes en ligne ou en quinconce. Les mesures de transfert thermique sont faites sur la base de rangée par rangée; les pressions sont mesurées à l'intérieur des bancs de tubes aussi bien qu'en amont et en aval. Le fluide de travail est l'air. Les visualisations montrent que le dérapage affecte fortement la façon d'attaquer les tubes par l'écoulement dans l'arrangement en ligne, avec un effet moindre dans l'arrangement en quinconce. Pour un nombre de Reynolds d'écoulement libre donné, le nombre de Nusselt diminue quand l'angle de dérapage augmente. L'effet du dérapage est bien corrélé pour l'arrangement en quinconce, mais pas aussi bien pour le cas en ligne à cause des modifications d'écoulement énoncées plus haut. Les nombres de Nusselt en ligne ne dépassent généralement pas ceux en quinconce et la perte de pression diminue quand le dérapage croît. Dans le domaine exploré, les pertes de charge en ligne sont plus faibles que celles en quinconce.

WÄRMEÜBERGANG, DRUCKVERLUST UND STRÖMUNGSFORMEN IN GENEIGETEN ROHRBÜNDELN

Zusammenfassung—Es wurden Experimente zur Ermittlung von Wärmeübergangs- und Druckverteilung und zur Sichtbarmachung von Strömungen durchgeführt, um den Einfluß der Rohrneigung bei versetzt und fluchtend angeordneten Rohrreihen zu untersuchen. Die Wärmeübergangsmessungen wurden reihenweise durchgeführt. Der Druck wurde sowohl innerhalb der Rohrreihen als auch stromauf- wie stromabwärts gemessen. Als Wärmeträgerfluid wurde Luft verwendet. Bei den optischen Untersuchungen zeigte sich, daß die Rohrneigung wesentlich das Aufprallverhalten der Strömung auf die Rohroberfläche im Fall der fluchtenden Anordnung beeinflußt, im Fall der versetzten Anordnung ist der Einfluß der Rohrneigung auf das Strömungsfeld weniger stark ausgeprägt. Bei gegebener Reynolds-Zahl in der Anströmung ist ein Abnehmen der Nusselt-Zahl mit zunehmenden Neigungswinkeln zu beobachten. Der Einfluß der Neigung konnte für die versetzte Anordnung gut korreliert werden, weniger gut für die fluchtende Anordnung aufgrund der oben beschriebenen Änderungen des Strömungsfeldes. Die Nusselt-Zahlen für die fluchtende Anordnung lagen meist über denen für die versetzte. Dieser Trend verstärkte sich bei stärkerer Neigung. Es konnte ein Abnehmen des Druckverlusts mit zunehmender Neigung festgestellt werden. Im untersuchten Arbeitsbereich lagen die Werte für den Druckverlust der fluchtenden Anordnung unter denen der versetzten Anordnung.

ТЕПЛООБМЕН, СОПРОТИВЛЕНИЕ И РЕЖИМЫ ТЕЧЕНИЯ ЖИДКОСТИ В ПУЧКАХ ТРУБ, РАСПОЛОЖЕННЫХ ПОД УГЛОМ К ПОТОКУ

Аннотация—Проведены эксперименты по исследованию сложного теплообмена, распределения давления и визуализации течения с целью изучения влияния угла наклона потока для шахматных и коридорных пучков труб. Измерения теплообмена проводились последовательно в каждом ряду труб, а давление измерялось внутри пучков, а также на входе и выходе из них. В качестве теплоносителя использовался воздух. Опыты по визуализации течения показали, что угол наклона потока оказывает заметное влияние на картину течения в коридорных пучках и несколько меньшее в шахматных. При заданном значении числа Рейнольдса число Нуссельта обычно уменьшалось с увеличением угла наклона. Влияние угла наклона хорошо поддается учету при шахматном расположении труб и несколько хуже при коридорном из-за отмеченных выше изменений в картине течения. Значения числа Нуссельта для коридорных пучков были выше соответствующих значений для шахматных, и это различие увеличивалось с увеличением угла наклона потока. Перепад давления уменьшался с увеличением угла наклона. В рассматриваемом диапазоне параметров измеренная разность давлений при коридорном расположении была меньше, чем при шахматном.